Recurrent activating mutations in *AHR* act as drivers of urinary tract cancer

Judith M. Vlaar[1], Anouska Borgman[2], Eric Kalkhoven[2], Nicolle Besselink[1], Charles Shale[3,4], Bishoy M. Faltas[5], Peter Priestley[3,4], Ewart Kuijk[1,6], Edwin Cuppen[1,3,6,7]

[1] Center for Molecular Medicine and Oncode Institute, University Medical Center Utrecht, the Netherlands.

[2] Center for Molecular Medicine, University Medical Center Utrecht, the Netherlands.

[3] Hartwig Medical Foundation, Amsterdam, The Netherlands.

[4] Hartwig Medical Foundation Australia, Sydney, New South Wales, Australia.

[5] Department of Medicine and Department of Cell and Developmental Biology, Weill Cornell Medicine, New York, NY, United States.

[6] Equal contribution

[7] contact: e.cuppen@hartwigmedicalfoundation.nl

Abstract

Bladder cancer is a common cancer with a high recurrence rate and with limited progress in treatment and survival of patients with advanced stages of the disease. The tumorigenesis of bladder cancer is still poorly understood, but identification of genetic contributors to its development may provide leads for targeted therapeutic approaches. By an in-depth analysis of whole-genome sequencing data of metastasized urinary tract cancer samples, we identified a novel recurrent in-frame deletion of exons 8 and 9 in the aryl hydrocarbon receptor (*AHR)* gene, encoding a ligand-activated transcription factor with context-specific physiological functions. The deletion ($AHR^{\Delta e8\text{-}9}$) is highly specific to urinary tract cancer and occurs in 10.7% of metastatic lesions. Additionally, a recurrent *AHR* hotspot point mutation and *AHR* gene amplifications were identified indicating that alterations in the *AHR* gene are a key cancer driver event for urinary tract cancer adding up to a prevalence of ~19% (40 out of 206).

The hotspot point mutation results in an amino acid change (AHR^{Q383H}) in the ligand-binding domain of the protein and causes altered ligand affinities such as AHR^{Q383H} activation upon incubation with the AhR antagonist CH-2233191. The in-frame deletion of exons 8 and 9 disrupt the ligand-binding domain and result in a constitutive nuclear localization of the protein and ligand-independent transcriptional activation. The constitutive activation of the AhR pathway by the $hAHR^{\Delta e8\text{-}9}$ mutant in mouse bladder organoids induces dedifferentiation and enables anchorage independent growth. In conclusion, our results indicate that AhR is a key proto-oncogene and cancer driver gene in urinary tract cancer and emphasize the potential of the AhR pathway as a target for therapeutic interventions.

Introduction

Bladder cancer is the fourth most common cancer in men with a 5-year survival rate of about 77% (American Cancer Society 2020). Despite risk stratification, the recurrence rate of bladder cancer is high and requires ongoing monitoring and treatment, which makes it also the costliest malignancy out of all cancers (James and Gore 2013). With recent advances, the therapeutic options have been expanded to include immune checkpoint inhibitors and antibody-drug conjugates, while clinical studies for targeted drug approaches are ongoing (Lenis et al. 2020; Loriot et al. 2019). However, treatment and overall survival of cases with advanced stages of bladder cancer have not really improved in the last decades as compared to other cancers and there remains a need for identification of drivers of bladder cancer tumorigenesis to effectively target early-stage disease and reduce tumor progression (Berdik 2017; Abdollah et al. 2013).

Genomic analyses of bladder cancer of various stages and grades have shown that bladder cancer is a heterogeneous disease of which the high mutation burden is largely driven by activation of APOBEC mutagenesis (Lawson et al. 2020; Nakauma-González et al. 2021; Robertson et al. 2018). Molecular characterization revealed activating *FGFR3* alterations in ~16% of the samples, with a higher prevalence in non-muscle invasive bladder cancer (Cancer Genome Atlas Research Network 2014; Robertson et al. 2018). Furthermore, positive selection of mutated genes in the RTK-Ras-PI3K pathway (such as *FGFR3*, *PIK3CA*, and *ERBB2*), the p53-Rb pathway (such as *TP53*, *RB1*, and *ATM*), and genes involved in chromatin remodeling (*KDM6A* and *KMT2D)* were identified in biopsies of patients with bladder cancer (Lawson et al. 2020; Robertson et al. 2018).

A recent study identified a rare non-synonymous mutation (Q383H) in *AHR* as an APOBEC-associated hotspot mutation in bladder cancer, suggesting *AHR* as a potential driver of bladder cancer (Shi et al. 2020). AhR is a ligand activated transcription factor involved in the cellular response to toxic aromatic hydrocarbons as well as cell type and context-specific physiologic functions (Denison et al. 2011). Increased *AHR* expression and activity have been associated with poor prognosis and survival for multiple cancers such as breast, lung, and upper urinary tract cancers (Wang et al. 2020). However, the relevance and functional consequences of cancer-associated *AHR* mutations in bladder cancer are poorly understood.

Here, we describe the identification of recurrent *AHR* alterations in the pan-cancer whole-genome sequencing database of metastatic cancers from Hartwig Medical Foundation. Using state-of-the-art data analysis tools with improved functionality for detecting structural variants

71 we identified a recurrent in-frame deletion of exons 8 and 9 in *AHR*. Together with the Q383H
72 point mutation and *AHR* gene amplifications, the variants comprise ~19% of patients with
73 urinary tract cancer. We demonstrate that the recurrent mutations lead to activated AhR
74 signaling and have transformation potential in mouse bladder organoids and may thus drive
75 urothelial tumorigenesis.

Results

AHR is frequently mutated in urinary tract cancers.

To identify genetic factors involved in urinary tract cancers, we analyzed the Hartwig database, which represents whole-genome sequencing data of solid metastatic tumors and normal tissue of 4500 patients (Priestley et al. 2019). Utilizing improved structural variant detection algorithms (Shale et al. 2020; Cameron et al. 2021), we detected a novel deletion spanning exons 8 and 9 of the *AHR* gene ($AHR^{\Delta e8\text{-}9}$) in 22 (10.7%) out of the 206 urinary tract samples (Fig. 1a, 1b). The $AHR^{\Delta e8\text{-}9}$ is identified in several urinary tract cancer subtypes, most of which are in bladder cancer (12/22) and pyelum (7/22) (Supplementary table 1). In the complete pan-cancer data set, the $AHR^{\Delta e8\text{-}9}$ mutant is identified in only three non-urinary tract samples, i.e. two lung cancer samples with a strong smoking signature and in a melanoma sample with a strong UV signature.

The identified exonic deletion was validated in RNA-sequencing data, which were available in the Hartwig database for a subset of the samples (129 out of 206 urinary tract samples). RNA sequencing read support for the *AHR* exon 7-10 splice junction is identified in all urinary tract samples harboring $AHR^{\Delta e8\text{-}9}$ (n = 16; Supplementary table 1). RNA read support for the *AHR* exon 7-10 splice junction also confirms the complete loss of exons 8 and 9 and the generation of an in-frame transcript for six samples in which the genomic start position of the deletion is located within the coding sequence of exon 8.

The deletion identified in *AHR* is relatively small (~ 3kb) with varying breakpoint locations per sample, which complicates its detection and may explain why it has not been described in previous studies (Robertson et al. 2018; ICGC/TCGA Pan-Cancer Analysis of Whole Genomes Consortium 2020). The 3' breakpoint junctions of most of the deletions are positioned in a narrow window of 30 bp between 2 Alu elements (AluYa5 and AluY) and overlap with the 3' site of the AluYa5 element (Fig. 1a). The Alu elements are orientated in opposite directions, contributing to a potential vulnerability of the DNA by ectopic invasion and annealing of the repetitive sequences of the Alu elements, a mechanism proposed to induce structural variation in cancer genes (Cook et al. 2020, 2013). Analysis of $AHR^{\Delta e8\text{-}9}$ in the RNA-sequencing data of an independent dataset of urinary tract cancers from Weill Cornell Medicine confirmed the presence of the 7-10 splice junction in 8% (2/24) of samples. One of the bladder cancer samples with the detected splice junction was of primary origin out of 8 primary tumors in this dataset (Supplementary table 3).

A targeted analysis of additional mutational events in the *AHR* gene in the Hartwig database resulted in the identification of gene amplifications and the Q383H point mutation (AHR^{Q383H}), in 16 (7.8%) and 2 (1.0%) of the urinary tract cancer samples, respectively (Fig. 1a, 1b). For

112 the samples with the genomic amplifications (n = 13), the gene expression (as measured by
113 the median adjusted TPM value from the RNA-seq data) is more than doubled compared to
114 the non-amplified urinary tract cancer samples (n = 100) indicating that the gene amplification
115 does result in increased gene expression (Fig. 1c). No RNA sequencing data was available
116 for the 2 samples with the identified AHR^{Q383H} hotspot point mutation.
117 The AHR^{Q383H} point mutation was previously reported as an APOBEC-associated hotspot
118 mutation in bladder cancer based on the TCGA PanCancer Atlas data (Shi et al. 2020). We
119 explored this mutagenic event in the TCGA PanCancer Atlas studies using the cBioportal
120 interface to study the incidence of the mutation in other cancer types (Gao et al. 2013; Cerami
121 et al. 2012). The AHR^{Q383H} point mutation was found in 11 samples out of almost 11,000
122 samples in the database, which are mainly of primary tumor origin. The vast majority (8)
123 occurred in bladder urothelial carcinomas samples with the other three in hepatocellular
124 carcinoma, papillary renal cell carcinoma, and lung adenocarcinoma. Thus, like the $AHR^{\Delta e8\text{-}9}$
125 in urinary tract data of the Hartwig database, the AHR^{Q383H} mutant is also highly specific for
126 urinary tract cancer.
127
128 We observed that *AHR* alterations are depleted with *FGFR3* alterations and *PIK3CA* mutations
129 among the urinary tract cancer samples in the Hartwig database (Fig. 1e). The depletion of
130 *FGFR3* alterations and *PIK3CA* mutations is most prominent for $AHR^{\Delta e8\text{-}9}$ although the
131 significance is impacted by low sample numbers (*FGFR3*: Odds ratio = 0.24 p = 0.21, *PIK3CA*:
132 Odds ratio = 0.30 p = 0.32). The tendency of mutual exclusivity with genes from the RTK-Ras-
133 PI3K pathway strengthens the idea of *AHR* as an independent driver and potential
134 convergence of AhR in this pathway. In addition, *AHR* alterations do not show depletion with
135 genes involved in chromatin remodeling or the tumor suppressors *TP53 and Rb1* (Fig. 1e,
136 Supplementary table 4).
137

138 ### The $hAHR^{Q383H}$ mutation affects ligand binding affinity and specificity

139 AhR belongs to the family of heterodimeric transcriptional regulators that contains a
140 bHLH/PAS motif (basic Helix-Loop-Helix/PER-ARNT-SIM), two PAS domains of which the
141 PAS-B domain contains the ligand binding domain (LBD) and a glutamine rich C-terminal site
142 (Fig. 1f) (Larigot et al. 2018; Denison et al. 2011). Inactive AhR is part of a multiprotein complex
143 containing two HSP90 molecules, one p23 molecule, and a XAP2 molecule that is localized
144 in the cytoplasm (Fig. 1g). Upon ligand binding, AhR dissociates from the multiprotein complex
145 and translocates to the nucleus where it forms a heterodimer with ARNT (Seok et al. 2017).
146 Part of the bHLH domains of the AhR/ARNT complex bind to XREs (Xenobiotic Response
147 Elements) consensus sequences in the genome to activate the transcription of a network of

genes of phase I and II drug metabolizing enzymes such as CYP1A1 and CYP1B1 (Denison et al. 2011).

The *AHR* point mutation (c.1149G>C) results in a glutamine to histidine substitution (AHR^{Q383H}), replacing a polar uncharged side chain with an aromatic ring. The crystal structure of the human and mouse AhR ligand-binding domain has not been described. However, homology-based modeling of the mouse AhR indicates that the mouse ortholog Ahr^{Q377} is part of the medial side of the mainly hydrophobic ligand binding cavity. It has been shown that the Q377 residue can form hydrogen bonds with AhR ligands in the ligand-binding domain and that introducing mutations that change this residue can affect ligand binding affinities (Xing et al. 2012; Pandini et al. 2007; Bisson et al. 2009).

To examine if the Q383H amino acid substitution alters the ligand-binding domain of the human AhR (hAHR) protein, we measured the transcriptional activity of $hAHR^{Q383H}$ and $hAHR^{WT}$ in a luciferase reporter assay. The hAHR constructs were expressed in combination with an XRE-luciferase reporter construct and the cells were subjected to different AhR ligands. Both the $hAHR^{WT}$ and $hAHR^{Q383H}$ cell lines showed strong transcriptional activity with AhR ligands TCDD and B[a]P (Fig. 2a). Stimulation with B[a]P resulted in a higher induction of luciferase transcription for the $hAHR^{Q383H}$ mutant than for the $hAHR^{WT}$, suggesting a difference in ligand affinity between both variants. The AhR antagonist CH-223191 inhibits TCDD binding to AhR and indeed the addition of CH-223191 to $hAHR^{WT}$ reduced transcriptional activation in the assay (Fig. 2a) (Kim et al. 2006; Zhao et al. 2010). Surprisingly, incubation of $hAHR^{Q383H}$ with CH-223191 resulted in transcriptional activation comparable to TCDD and no obvious antagonism when tested in combination with TCDD or B[a]P (Fig. 2a). To examine this altered ligand-binding specificity, we analyzed the protein localization of $hAHR^{Q383H}$ and $hAHR^{WT}$ in RPE1 cells expressing the constructs. In the absence of a ligand, both $hAHR^{Q383H}$ and $hAHR^{WT}$ proteins are mainly localized in the cytoplasm and both proteins show nuclear localization upon incubation with TCDD or B[a]P (Fig. 2c, Supplementary fig. 1). Incubation with the antagonist CH-223191 however resulted in a clear nuclear localization of $hAHR^{Q383H}$, while the $hAHR^{WT}$ remains localized in the cytoplasm (Fig. 2c). The difference in responses between the $hAHR^{Q383H}$ and $hAHR^{WT}$ to the antagonist CH-223191 and seemingly to B[a]P demonstrates distinctive ligand binding properties of the Q383H mutant, thereby sensitizing cells to AhR pathway stimulation.

181

182 The $hAHR^{\Delta e8-9}$ mutant leads to constitutive AhR pathway activation

183 The deletions identified in the *AHR* gene result in the loss of exons 8 and 9. At the protein
184 level, this results in an in-frame protein coding sequence with the loss of 84 amino acids (p.
185 303-387), disrupting the PAS-B domain and the C-terminal part of the ligand-binding domain
186 of the protein. The HSP90 and XAP2 protein binding domains are predicted to be affected,
187 while the dimerization region of the protein likely remains intact (Fig. 1g).
188

189 To study the functional consequences of $AHR^{\Delta e8-9}$, we created transgenic $hAHR^{\Delta e8-9}$ RPE1
190 cells and mouse bladder organoids. In contrast with the expression of $hAHR^{WT}$, the $hAHR^{\Delta e8-}$
191 ^{9} is localized in the nucleus regardless of the presence or absence of a ligand (Fig. 2c).
192 Expression of the hAHR mutants in mouse bladder organoids confirmed aberrant ligand-
193 independent nuclear localization of the $hAHR^{\Delta e8-9}$ mutant (Fig. 2d). Together, these findings
194 show that disruption of the ligand-binding domain and PAS-B domain by loss of exons 8 and
195 9 causes constitutively nuclear localization of $hAHR^{\Delta e8-9}$.
196

197 We performed the XRE-luciferase reporter assay to examine whether $hAHR^{\Delta e8-9}$ can still
198 promote transcriptional activation. The transcriptional activation activity of $hAHR^{\Delta e8-9}$ was
199 similar for all the conditions, irrespective of the presence of AhR ligands. The addition of the
200 AhR antagonist CH-223191 also did not affect the transcriptional activation activity of $hAHR^{\Delta e8-}$
201 ^{9} (Fig. 2a). Increased concentrations of $hAHR^{WT}$ and $hAHR^{\Delta e8-9}$ constructs in the transfections
202 resulting in increased expression levels, revealed that $hAHR^{\Delta e8-9}$ induces higher transcriptional
203 activity levels than $hAHR^{WT}$ in untreated conditions (Fig. 2b).
204

205 To determine the consequences of the constitutively activated $hAHR^{\Delta e8-9}$ on the transcriptome
206 we performed RNA-sequencing on the mouse bladder organoids. The untreated organoids
207 expressing $hAHR^{\Delta e8-9}$ differentially expressed several genes compared to the untreated
208 organoids expressing $hAHR^{WT}$, including the AhR target genes *Cyp1a1, Cyp1b1, Ahrr, Gsta1,*
209 and *Tiparp* demonstrating activation of the canonical AhR pathway (Fig. 3a). The expression
210 pattern of up and down regulated genes is similar for $hAHR^{\Delta e8-9}$ in untreated and TCDD treated
211 conditions. The activation of the AhR target genes is also observed in the RNA-sequencing
212 data of the urinary tract cancer samples carrying the $AHR^{\Delta e8-9}$ mutation in the Hartwig
213 database (Fig. 1d). Upregulation of the canonical AhR target genes in the cancer samples
214 harboring $AHR^{\Delta e8-9}$ but not in the AhR amplified or AhR non-affected samples demonstrates
215 that the AhR pathway is constitutively activated in these samples.
216

The organoids expressing hAHR^{WT} treated with TCDD also show upregulation of the canonical AhR target genes but do not show the same downregulated genes (Fig. 3a). This observation indicates a different effect on the transcriptome between the constitutive active hAHR$^{\Delta e8\text{-}9}$ and the 24 hours TCDD activated hAHR^{WT} condition. Moreover, the comparison of the expression of the AhR target genes between organoids that express the hAHR mutants and the control organoids indicates that overexpression of hAHR^{WT} and hAHR^{Q383H} without the addition of exogenous ligand already results in modest pathway activation (Fig. 3b). These observations are in line with the higher induction of luciferase transcription in the untreated condition for the hAHR^{WT} and hAHR^{Q383H} constructs compared to the control in the luciferase assay (Fig. 2a).

We performed GO enrichment analysis on all differentially expressed genes in the mouse organoid models to understand which pathways and processes are potentially affected by the long-term activation of hAHR$^{\Delta e8\text{-}9}$. Most outstanding is the enrichment of downregulated genes related to the extracellular matrix and cell periphery organization in the cellular component domain (Fig. 3c, Supplementary table 5). The bladder is a stratified epithelium, with stem cells that reside in the basal cell layer that support organ regeneration and renewal. Upon differentiation, the stem cells give rise to intermediate cells and luminal umbrella cells that are fully differentiated and form an impenetrable barrier. Mouse organoids expressing hAHR$^{\Delta e8\text{-}9}$ show downregulation of the differentiated luminal cell markers *Upk3a*, *Upk1a*, and *Krt18* and upregulation of the basal proliferative markers *Krt6b, Wnt5a*, and *Krt1* when compared to organoids expressing hAHR^{WT} (Fig. 3d) (Santos et al. 2019; Z. Yu et al. 2019; Guo et al. 2020). Santos et al. showed that mouse bladder organoids enriched for undifferentiated basal cells have a reduced diameter of the lumen and increased thickness of the epithelial layer when compared to organoids composed of more differentiated intermediate and umbrella cells (Santos et al. 2019). We observed a mixture of cystic and compact organoids in the mouse bladder organoids expressing hAHR^{WT}, indicating the presence of both differentiated and undifferentiated cell types. No cystic organoids were observed in the organoids expressing hAHR$^{\Delta e8\text{-}9}$ indicating a less differentiated phenotype (Fig. 3e). To explore if hAHR$^{\Delta e8\text{-}9}$ not only induces a stem cell phenotype but also contributes to oncogenic transformation, a soft agar growth assay was performed. A higher number of colonies were counted for the organoids expressing hAHR$^{\Delta e8\text{-}9}$ compared to the organoids expressing hAHR^{WT} or control organoids demonstrating that hAHR$^{\Delta e8\text{-}9}$ confers anchorage-independent growth to bladder cells (Fig. 3f). Together, these observations demonstrate that hAHR$^{\Delta e8\text{-}9}$ leads to constitutive activation of the AhR pathway in mouse bladder organoids resulting in a transformation of cells towards a less differentiated phenotype that is able to grow independent of anchorage to the extracellular matrix.

Discussion

In this study, we discovered a novel recurrent deletion in the *AHR* gene with a high prevalence in urinary tract cancer samples. *AHR* is also affected by a hotspot mutation (Q383H) as well as copy number amplifications in this cancer type. With functional studies, we show that the *AHR* alterations activate the canonical AhR pathway and AhR signaling and thereby modulate transcriptional expression. In particular, $hAHR^{Q383H}$ leads to more sensitized ligand-dependent activation while $hAHR^{\Delta e8\text{-}9}$ leads to ligand-independent constitutive activation of the AhR pathway thereby promoting bladder cells to adopt a transformed undifferentiated proliferative phenotype allowing anchorage-independent growth. This is in line with previous work showing that *AHR* overexpression can lead to malignant transformation of epithelial cells and the oncogenic potential of constitutively activated AhR in mice (Brooks and Eltom 2011; Andersson et al. 2002; Dantsuka et al. 2019).

The high prevalence of ~10% of the $AHR^{\Delta e8\text{-}9}$ in metastasized urinary tract cancers and the identification of the event in primary tumors, indicates a high positive selection pressure of this structural variant alteration and our findings suggests *AHR* as a prevalent novel driver event in urinary tract cancer. The incidence of the AHR^{Q383H} point mutation in our dataset is low although it is a clear hotspot mutation that is strongly enriched in urinary tract cancers of the TCGA dataset on cBioportal (Cerami et al. 2012; Gao et al. 2013). In contrast with $hAHR^{\Delta e8\text{-}9}$, the $hAHR^{Q383H}$ depends on stimulation by ligands. We demonstrate that $hAHR^{Q383H}$ leads to increased sensitivity which may also lead to overactivity of the AhR pathway in the urinary tract, thereby driving tumorigenesis. This likely also holds true for *AHR* amplifications since overexpression of $hAHR^{wt}$ in different models shows a modest increase of AhR pathway activation compared to the controls. It is not yet known if the ligands that induce overactive AhR signaling in the *AHR* amplified and AHR^{Q383H} backgrounds are of environmental origin (like components in tobacco smoke) or have an endogenous source (like endogenous metabolites) (Denison and Nagy 2003). Surprisingly, we observed $hAHR^{Q383H}$ activation upon treatment with the AhR antagonist CH-223191. This contrasts with a recent study that demonstrated reduced viability upon treatment with CH-223191 of the bladder cancer cell line KMBC2 harboring the AHR^{Q383H} mutation (Shi et al. 2020). A possible explanation for the apparent discrepancy in results may lie in the different types of experiments that were conducted and it also remains to be demonstrated if the reduced viability of the KMBC2 cell line after CH-223191 incubation is due to reduced or increased AhR pathway activity.

A variety of molecular signaling pathways have been linked previously to AhR-mediated tumor initiation, tumor promotion, and tumor progression whether or not in a cancer type-specific

290 background and/or driven by AhR agonists (Dietrich and Kaina 2010; Wang et al. 2020). This
291 includes the biotransformation of hydrocarbons by CYP enzymes to mutagenic intermediates
292 which can induce DNA adducts, cross-talk of AhR with other signaling pathways, and
293 interaction of AhR with other binding partners than ARNT to promote transcription of non-
294 canonical genes (Shimizu et al. 2000; Wilson, Joshi, and Elferink 2013; Vogel et al. 2011; Xie,
295 Peng, and Raufman 2012; Fritsche et al. 2007; Baker, Sakoff, and McCluskey 2020). The
296 underlying molecular signaling pathways driving the tumorigenesis of urinary tract cancers in
297 patients with activating mutations in *AHR* remains unclear. The tendency of mutual exclusivity
298 between *AHR* and *FGFR3,* and *AHR*$^{\Delta e8\text{-}9}$ *and PIK3CA* may indicate convergence on the same
299 pathway, although a fully independent parallel oncogenic pathway in bladder cancer driven by
300 AhR can not be excluded. Our results, nor information in literature, provides clues why AhR
301 activation is so specific for bladder cancer, so this will require further investigations. We
302 demonstrate that the mouse bladder organoids recapitulate AhR activating mechanisms and
303 thus provide a versatile tissue-specific *in vitro* model to further elucidate the underlying
304 oncogenic signaling pathways and mechanisms.
305
306 Patients that harbor AhR activating mutations could potentially benefit from AhR targeted
307 therapies (Kolluri, Jin, and Safe 2017). Here we show that the mode of action of AhR activation
308 differs between the different mutations, which implies that tailored therapies depending on the
309 underlying mutational event are required. Most classic AhR antagonists function by
310 interference with the ligand-binding domain, but this domain is not targetable for the AHR$^{\Delta e8\text{-}9}$
311 mutant as this domain is deleted. Therefore, functional screens to identify specific AHR$^{\Delta e8\text{-}9}$
312 targeting compounds or the identification of essential downstream activated processes could
313 be a next step towards the identification of novel treatment strategies for selected urinary tract
314 cancer patients in the context of precision medicine.

Material and Methods

Driver gene status urinary tract cohort

Variant detection and driver likelihood status are based on the Hartwig database (Priestley et al. 2019). Driver likelihood is introduced to select for a sample specific likelihood of each gene based on the type of variant and taking the mutation load per sample into account. To select for affected genes in the urinary tract cancer samples, the driver likelihood score is set to > 0.8 and detected gene fusions with a high impact are included. Visualized are the genes affected in more than 12.5% of the samples (top 12 genes). Mutually exclusivity is pairwise calculated with Fisher Exact Test based on Odd Ratio cut-offs as described in Gao et al. (Gao et al. 2013).

Gene constructs

An expression plasmid containing the *AHR* WT sequence was purchased from Origene (RC209832). The Q383H point mutation was introduced with site-directed mutagenesis protocol with forward primer cattgtaactcacagaccactaacagatg and reverse primer gttagtggtctgtgagttacaatgatataatc. The AHR WT, AHR Q383H, and AHR DelExon sequences were cloned in a lentiviral plasmid (Addgene #52961) and subsequently to pcDNA3.1 vector with the In-fusion HD Eco-dry cloning (Takarabio) following manufacturer's protocol. Primers for lentiviral plasmid are: forward N-flag caggaccggttctaggatatcgccaccatggattacaaagacgatgacgataagaacagcagcagcgccaac, forward caggaccggttctaggatatcgccaccatgaacagcagcagcgcc, reverse ttgttgcgccggatcgcaggaatccactggatgtcaaatcag, reverse C-flag ttgttgcgccggatcgcttatcgtcatcgtctttgtaatccaggaatccactggatgtcaaatcag, forward deletion tggttgtgatgccaaagatgaggaaggaacagagca and reverse deletion gttccttcctcatctttggcatcacaaccaatagg. Primers cloning of AhR sequences to pcDNA3.1 vector are forward taccgagctcggatcatatcgccaccatgaacag and reverse gatatctgcagaattttacaggaatccactggatgtcaaat.

The luciferase reporter vector pGL3-XRE-Luc2 reporter vector was constructed with two mutagenesis steps with an in-house pGL3-minP-Luc2 vector containing DNA binding sequence “gggaggtacttggagcggc” with primers forward-1 gcgtgctagcccgggTTGCGTGACCctcgagatctgcgat, reverse-1 atcgcagatctcgagGGTCACGCAAcccgggctagcacgc, forward-2 aatcgataaggatccTTGCGTGACCgtcgaccgatgccct, reverse-2 agggcatcggtcgacGGTCACGCAAggatccttatcgatt.

350 Cell culture

351 All cells were cultured in a humidified atmosphere at 37 °C under 5% CO_2 and 20% O_2.
352 Lentivirus particles containing AHR constructs were produced by transient calcium phosphate
353 transfection of HEK293T. Virus particles were concentrated with Lenti-X Concentrator
354 (Takarabio) according to the manufacturer's directions.
355
356 Mouse bladder organoids were a kind gift from dr. Hans Clevers and were cultured as
357 previously reported with minor adaptations (Mullenders et al. 2019). In short, mouse bladder
358 organoids were plated in droplets of ice-cold Matrigel (Corning). After the matrigel had
359 solidified, a complete mouse bladder medium was added consisting of Advanced DMEM/F-12
360 supplemented with HEPES, Glutamax, 1% penicillin, 1% streptomycin, Nicotinamide (10 mM),
361 N-Acetylcysteine (1.25 mM), FGF10 (100 ng/mL of Peprotech 100-26), FGF7 (25 ng/mL of
362 Peprotech 100-19), A83-01 (500 nM), B27 (ThermoFisher 17504001) and primocin
363 (Invivogen). Organoids were passaged weekly either through mechanical shearing with a
364 pulled Pasteur's pipet or by dissociation using TrypLE. To increase survival the medium was
365 supplemented with ROCK inhibitor (Y-27632, 10 μM) after passaging.
366
367 hTERT RPE1 and HEK293T cells were cultured in DMEM, 10% fetal bovine serum, 1%
368 penicillin, and 1% streptomycin. For virus transduction and range of volume of the virus was
369 added to hTERT RPE1 cells and the mouse bladder organoids to their growth medium
370 supplement with polybrene. hTERT RPE1 cells and the mouse bladder organoids were placed
371 on 10-15 μg/ml and 1 μg/ml puromycin selection, respectively.
372
373 Cells were incubated with 10 nM TCDD (LGC), 10 μM B[a]P (sigma), or 10 μM CH-223191
374 (Sanbio) or vehicle alone (DMSO) for 24 hours unless otherwise stated.
375

376 Immunofluorescence

377 RPE1 cells expressing hAHR mutants were plated on coverslips and incubated with TCDD,
378 B[a]P, CH-223191 or untreated (DMSO) for 4 or 24 hours. Cells were fixed in 4%
379 formaldehyde, permeabilized with 0.3% Triton X-100 in PBS, and blocked with 4% BSA in
380 PBS. AhR was stained with Anti-Aryl hydrocarbon Receptor antibody (Abcam ab190797) in
381 the blocking buffer. After incubation with the primary antibody, the cells were washed followed
382 by incubation with secondary antibody conjugated with Alexa fluor dyes. Subsequently, the
383 cells were washed, counterstained with DAPI, and mounted on microscope slides. Images
384 were taken with predefined settings on Zeiss LSM510 microscope and analyzed with
385 Fuij/imageJ. Ratios of AhR signal intensities were calculated by determining average grey

386 value intensities for each nucleus, based on dapi staining, and for each corresponding
387 cytoplasm, as 1μM band around each nucleus.
388
389 The first steps in the immunofluorescence procedure for the mouse bladder organoids are
390 different from the procedure described previously. First, dispase was added to a final
391 concentration of 1mg/ml to a warm medium and incubated for 30 min at 37°C to dissolve the
392 Matrigel. Organoids were harvested by gentle pipetting, collected in a tube, and washed with
393 cold Advanced DMEM/F12. The organoids were centrifuged, washed in PBS followed by
394 another centrifugation step. The resulting organoid pellet was resuspended in 100 µl PBS and
395 transferred to a Lab-Tek Chamber slide well. The organoids were fixed by the addition of 4%
396 formaldehyde followed by 1h incubation at RT. The organoids attached to the bottom of the
397 chamber slide were washed twice with PBS. Subsequently, the organoids were incubated in
398 the blocking buffer and the remaining immunofluorescence procedure was followed as
399 described for the RPE1 cells.

400 Luciferase reporter gene assay

401 HEK293T cells were cultured in a 24-wells plate and transiently transfected with pcDNA3.1
402 empty vector or pcDNA3.1 vector containing the expression cassette of $hAHR^{WT}$, $hAHR^{Q383H}$,
403 or $hAHR^{\Delta e8\text{-}9}$ (10 ng), together with the pGL3-XRE-Luc2 reporter vector (1000 ng) and pRL-
404 CMV Renilla vector (2 ng). 24 hours after transfection, cells were treated with ligand TCDD
405 (50 nM) or B[a]P and/or antagonist CH223191 for approximately 24 hours. Luciferase activity
406 was measured with the Dual-Luciferase reporter assay system and normalized for Renilla
407 activity (Promega, Madison, WI). The results are averages of at least three independent
408 experiments assayed in duplicate ± SEM. Results are presented as change relative to the
409 empty vector in the untreated (DMSO) condition.

410 RNA-sequencing

411 The RNA from the transgenic mouse bladder organoids was isolated with Trizol
412 (ThermoFisher) according to the manufacturer's instructions. RNA-seq libraries were prepared
413 using TruSeq Stranded Total RNA Library Prep Kit (Illumina) according to the manufacturer's
414 protocol. RNA-seq libraries were pooled and sequenced on a NextSeq2000 (Illumina) in
415 1x50bp single end mode. RNA sequencing reads were aligned against mouse reference
416 genome GRCm38 using STAR and the number of reads mapping to genes was counted using
417 featureCounts all by using a custom in-house pipeline
418 (https://github.com/UMCUGenetics/RNASeq-NF). The Bioconductor package DESeq2 was
419 used to normalize raw read counts and to perform differential gene expression analysis with
420 apeglm shrinkage (Love, Huber, and Anders 2014; Zhu, Ibrahim, and Love 2019). The

421 analyses were performed with significant (P.adjust <0.05) and differentially expressed
422 (Log2FoldChange >2.5) genes with exception of luminal and basal marker analyses where
423 smaller differences were included (Log2FoldChange > 1.5). The Bioconductor package
424 clusterProfiler and Revigo were used for the GO enrichment analysis (G. Yu et al. 2012; Supek
425 et al. 2011).

426 ### Soft agar assay

427 For the soft agar assay, 3% agarose (REF 11388991001) was dissolved and autoclaved in
428 100 ml EBSS supplemented with HEPES. One volume of melted 3% agarose was mixed with
429 four volumes of Advanced DMEM F12 supplemented with HEPES, Glutamax, 1% penicillin,
430 and 1% streptomycin to obtain 0.6% solution. This mixture was added to 6-well plates (1.5
431 ml/well) in which the gels were allowed to solidify. Subsequently, Tryple was used to prepare
432 single-cell suspensions of the mouse bladder organoids. The cells were counted and for each
433 condition, 2.5 ml of cell suspension was prepared at a concentration of $1x10^{e4}$ cells/ml in
434 complete medium. The cell suspension was warmed to 37°C and subsequently mixed 1:1 with
435 a warm 0.6% agarose solution to get $0.5\ x10^{e4}$ cells/ml in 0.3% agarose solution. Per well 1.5
436 ml agarose/cell mixture was plated. Plates were allowed to settle at RT for 1h followed by 15
437 min at 4°C before being placed in a tissue culture incubator. The next day 300 µl of the medium
438 was added and the cells were refed every 2 - 4 days. After 3 weeks the cells were stained with
439 nitroblue tetrazolium chloride solution. Colonies were counted using ImageJ software.

440 ## Figures

441 Figure 1. *AHR* alterations in somatic metastatic urinary tract samples.
442 **a.** Schematic representation of *AHR* gene (ENST00000242057.4 - GRCh37) with a
443 magnification of the genomic region around exon 7 - 9 (Chr7:17372389-17378532). The point
444 mutation Q383H (c.1149G>C) is marked with an asterisk. The black bars in the lower part of
445 the figure represent the extent of the genomic deletions identified in the urinary tract cancer
446 samples. See supplementary table 2 for genomic positions of the deletions. **b.** Pie chart of the
447 number of detected *AHR* alterations: *AHR* amplification (Amp), $AHR^{\Delta e8\text{-}9}$, AHR^{Q383H} or non-
448 affected samples in the urinary tract samples of the Hartwig database. **c.** Boxplot of the
449 adjusted TPM values for AHR transcript. Asterisks indicate two samples that contain the
450 deletion ($AHR^{\Delta e8\text{-}9}$) but also have an amplification of the *AHR* gene. **d.** Boxplot of the adjusted
451 TPM values of AhR target genes. **e.** Visualization of top 12 affected genes per mutation type
452 in urinary tract cancer samples of the Hartwig database (Priestley et al. 2019). Gene names
453 are colored for oncogenes (red) and tumor suppressor genes (blue). **f.** Schematic illustration
454 of the AhR functional domains and the positions of AHR^{Q383H} and $AHR^{\Delta e8\text{-}9}$. The deletion
455 ($AHR^{\Delta e8\text{-}9}$) disrupts the PAS-B domain, ligand-binding domain (LBD), and XAP2 and HSP90

456 protein interaction domains. **g.** Canonical AhR signaling pathway. Created with
457 BioRender.com.
458
459 Figure 2. Altered protein localization and mediated transcription activation of hAHR mutants.
460 **a.** Luciferase reporter assay of HEK293T cells transfected with empty control, $hAHR^{WT}$,
461 $hAHR^{Q383H}$, or $hAHR^{\Delta e8\text{-}9}$ vectors together with XRE-luciferase reporter construct. Assays were
462 performed with different AhR ligands (TCDD and B[a]P) and AhR antagonist (CH-223191)
463 conditions. Significance was calculated with Student's T-test for stimulated versus untreated
464 condition per construct. * $p < 0.05$, ** $p < 0.01$. RLU = relative luciferase unit. **b.** Luciferase
465 reporter assay of HEK293T cells transfected with increasing concentration of $hAHR^{WT}$,
466 $hAHR^{\Delta e8\text{-}9}$, and empty control vectors. **c.** Immunofluorescence of RPE1 cells that express
467 $hAHR^{WT}$, $hAHR^{Q383H}$, or $hAHR^{\Delta e8\text{-}9}$ that were incubated for 4 hours with TCDD or CH-223191.
468 AhR was detected with immunofluorescence (red) and DNA with Dapi (blue). The boxplots
469 present the AhR signal ratio of nuclear to cytoplasmic signal for all individual captured cells.
470 **d.** Immunofluorescence of mouse bladder organoids that express $hAHR^{WT}$, $hAHR^{Q383H}$, or
471 $hAHR^{\Delta e8\text{-}9}$ and were incubated for 24 hours with TCDD. AhR was detected with
472 immunofluorescence (red) and DNA with Dapi (blue).
473
474 Figure 3: Transcriptome analysis of constitutively activated $hAHR^{\Delta e8\text{-}9}$ mutant.
475 **a.** Rlog values of the 172 most differentially expressed genes between the $hAHR^{WT}$ and
476 $hAHR^{\Delta e8\text{-}9}$ expressing mouse bladder organoids in untreated and TCDD treated conditions. **b.**
477 Boxplot of normalized counts of RNA reads of AhR target genes for the untreated mouse
478 bladder organoids expressing hAHR mutants (n=4). **c.** GO enrichment analysis of $hAHR^{\Delta e8\text{-}9}$
479 mutant for the cellular component domain. **d.** Rlog values of basal and luminal cell layer
480 makers for $hAHR^{\Delta e8\text{-}9}$ and $hAHR^{WT}$ expressing mouse bladder organoids. **e.** Images of Dapi
481 stained mouse bladder organoids expressing hAHR mutants. The lower panel shows the
482 magnification of the boxed area. Scale bar 250 µm. **f.** Soft agar assay of mouse bladder
483 organoids expressing hAHR mutants. Results are presented as the mean ± SD of triplicate
484 samples.

485 ## Supplementary information

486 Supplementary table 1: Overview urinary tract cancer data HMF database
487 Supplementary table 2: Overview $AHR^{\Delta e8\text{-}9}$ breakpoint information
488 Supplementary table 3: AHR RNA-seq splice junction detection in urinary tract cancers of Weill
489 Cornell Medicine
490 Supplementary table 4: Selected driver genes in urinary tract cancer samples based on
491 Hartwig database.

492 Supplementary table 5: GO enrichment analysis details of mouse bladder organoids
493 expressing hAHR$^{\Delta e8\text{-}9}$
494
495 Supplementary figure 1: AHR protein localization after incubation with B[a]P or CH-223191.
496 Immunofluorescence of RPE1 cells that express hAHR^{WT}, hAHR^{Q383H}, or hAHR$^{\Delta e8\text{-}9}$ that were
497 incubated for 4 hours with B[a]P or with AhR antagonist CH-223191. AhR was detected with
498 immunofluorescence (red) and DNA with Dapi (blue). The boxplots present the AhR signal
499 ratio of nuclear to cytoplasmic signal for all individual captured cells.

500 Acknowledgments

501 We thank Utrecht Sequencing Facility for providing sequencing service and the UMC Utrecht
502 Bioinformatics Expertise Core for data analysis and data handling. Utrecht Sequencing Facility
503 is subsidized by the University Medical Center Utrecht, Hubrecht Institute, Utrecht University,
504 and The Netherlands X-omics Initiative (NWO project 184.034.019). The UMC Utrecht
505 Bioinformatics Expertise Core is subsidized by the University Medical Center Utrecht, Center
506 for Molecular Medicine. This publication and the underlying study have been made possible
507 partly based on the data that Hartwig Medical Foundation and the Center of Personalised
508 Cancer Treatment (CPCT) have made available to the study.

509 Author contributions

510 JMV, E. Kuijk, NB and EC designed and performed experiments including data analysis and
511 interpretation. AB, and E Kalkhoven designed and performed the luciferase assay
512 experiments. CS and PP conducted Hartwig database analysis. BMF provided Weill Cornell
513 Medicine data analysis. PP and EC conceived the original idea. EC and E Kuijk supervised
514 the project. JMV, E Kuijk, and EC wrote the manuscript with input from all authors.

515 Competing interests

516 The authors declare no competing interests.

517 References

518 Abdollah, Firas, Giorgio Gandaglia, Rodolphe Thuret, Jan Schmitges, Zhe Tian, Claudio
519 Jeldres, Niccolò Maria Passoni, et al. 2013. “Incidence, Survival and Mortality Rates of
520 Stage-Specific Bladder Cancer in United States: A Trend Analysis.” *Cancer*
521 *Epidemiology* 37 (3): 219–25.
522 Andersson, Patrik, Jacqueline McGuire, Carlos Rubio, Katarina Gradin, Murray L. Whitelaw,
523 Sven Pettersson, Annika Hanberg, and Lorenz Poellinger. 2002. “A Constitutively Active
524 Dioxin/aryl Hydrocarbon Receptor Induces Stomach Tumors.” *Proceedings of the*
525 *National Academy of Sciences of the United States of America* 99 (15): 9990–95.
526 American Cancer Society. Cancer Facts & Figures 2020. Atlanta: American Cancer Society;

527 2020.
528 Baker, Jennifer R., Jennette A. Sakoff, and Adam McCluskey. 2020. “The Aryl Hydrocarbon
529 Receptor (AhR) as a Breast Cancer Drug Target.” *Medicinal Research Reviews* 40 (3):
530 972–1001.
531 Berdik, Chris. 2017. “Unlocking Bladder Cancer.” *Nature* 551 (7679): S34–35.
532 Bisson, William H., Daniel C. Koch, Edmond F. O’Donnell, Sammy M. Khalil, Nancy I.
533 Kerkvliet, Robert L. Tanguay, Ruben Abagyan, and Siva Kumar Kolluri. 2009. “Modeling
534 of the Aryl Hydrocarbon Receptor (AhR) Ligand Binding Domain and Its Utility in Virtual
535 Ligand Screening to Predict New AhR Ligands.” *Journal of Medicinal Chemistry*.
536 Brooks, J., and S. E. Eltom. 2011. “Malignant Transformation of Mammary Epithelial Cells by
537 Ectopic Overexpression of the Aryl Hydrocarbon Receptor.” *Current Cancer Drug*
538 *Targets* 11 (5): 654–69.
539 Cameron, Daniel L., Jonathan Baber, Charles Shale, Jose Espejo Valle-Inclan, Nicolle
540 Besselink, Arne van Hoeck, Roel Janssen, Edwin Cuppen, Peter Priestley, and Anthony
541 T. Papenfuss. 2021. “GRIDSS2: Comprehensive Characterisation of Somatic Structural
542 Variation Using Single Breakend Variants and Structural Variant Phasing.” *Genome*
543 *Biology* 22 (1): 202.
544 Cancer Genome Atlas Research Network. 2014. “Comprehensive Molecular
545 Characterization of Urothelial Bladder Carcinoma.” *Nature* 507 (7492): 315–22.
546 Cerami, Ethan, Jianjiong Gao, Ugur Dogrusoz, Benjamin E. Gross, Selcuk Onur Sumer,
547 Bülent Arman Aksoy, Anders Jacobsen, et al. 2012. “The cBio Cancer Genomics Portal:
548 An Open Platform for Exploring Multidimensional Cancer Genomics Data.” *Cancer*
549 *Discovery* 2 (5): 401–4.
550 Cook, George W., Michael G. Benton, Wallace Akerley, George F. Mayhew, Cynthia
551 Moehlenkamp, Denise Raterman, Daniel L. Burgess, et al. 2020. “Structural Variation
552 and Its Potential Impact on Genome Instability: Novel Discoveries in the EGFR
553 Landscape by Long-Read Sequencing.” *PloS One* 15 (1): e0226340.
554 Cook, George W., Miriam K. Konkel, Jerilyn A. Walker, Matthew G. Bourgeois, Mitchell L.
555 Fullerton, John T. Fussell, Heath D. Herbold, and Mark A. Batzer. 2013. “A Comparison
556 of 100 Human Genes Using an Alu Element-Based Instability Model.” *PloS One* 8 (6):
557 e65188.
558 Dantsuka, Ai, Osamu Ichii, Annika Hanberg, Yaser Hosny Ali Elewa, Saori Otsuka-
559 Kanazawa, Teppei Nakamura, and Yasuhiro Kon. 2019. “Histopathological Features of
560 the Proper Gastric Glands in FVB/N-Background Mice Carrying Constitutively-Active
561 Aryl-Hydrocarbon Receptor.” *BMC Gastroenterology* 19 (1): 102.
562 Denison, Michael S., and Scott R. Nagy. 2003. “Activation of the Aryl Hydrocarbon Receptor
563 by Structurally Diverse Exogenous and Endogenous Chemicals.” *Annual Review of*
564 *Pharmacology and Toxicology* 43: 309–34.
565 Denison, Michael S., Anatoly A. Soshilov, Guochun He, Danica E. DeGroot, and Bin Zhao.
566 2011. “Exactly the Same but Different: Promiscuity and Diversity in the Molecular
567 Mechanisms of Action of the Aryl Hydrocarbon (dioxin) Receptor.” *Toxicological*
568 *Sciences: An Official Journal of the Society of Toxicology* 124 (1): 1–22.
569 Fritsche, Ellen, Claudia Schäfer, Christian Calles, Thorsten Bernsmann, Thorsten
570 Bernshausen, Melanie Wurm, Ulrike Hübenthal, et al. 2007. “Lightening up the UV
571 Response by Identification of the Arylhydrocarbon Receptor as a Cytoplasmatic Target
572 for Ultraviolet B Radiation.” *Proceedings of the National Academy of Sciences of the*
573 *United States of America* 104 (21): 8851–56.
574 Gao, Jianjiong, Bülent Arman Aksoy, Ugur Dogrusoz, Gideon Dresdner, Benjamin Gross, S.
575 Onur Sumer, Yichao Sun, et al. 2013. “Integrative Analysis of Complex Cancer
576 Genomics and Clinical Profiles Using the cBioPortal.” *Science Signaling* 6 (269): l1.
577 Guo, Charles C., Jolanta Bondaruk, Hui Yao, Ziqiao Wang, Li Zhang, Sangkyou Lee, June-
578 Goo Lee, et al. 2020. “Assessment of Luminal and Basal Phenotypes in Bladder
579 Cancer.” *Scientific Reports* 10 (1): 9743.
580 ICGC/TCGA Pan-Cancer Analysis of Whole Genomes Consortium. 2020. “Pan-Cancer
581 Analysis of Whole Genomes.” *Nature* 578 (7793): 82–93.

James, Andrew C., and John L. Gore. 2013. “The Costs of Non-Muscle Invasive Bladder Cancer.” *The Urologic Clinics of North America* 40 (2): 261–69.

Kim, Sun-Hee, Ellen C. Henry, Dong-Kyu Kim, Yun-Hee Kim, Kum Joo Shin, Myoung Sook Han, Taehoon G. Lee, et al. 2006. “Novel Compound 2-Methyl-2H-Pyrazole-3-Carboxylic Acid (2-Methyl-4-O-Tolylazo-Phenyl)-Amide (CH-223191) Prevents 2,3,7,8-TCDD-Induced Toxicity by Antagonizing the Aryl Hydrocarbon Receptor.” *Molecular Pharmacology*. https://doi.org/10.1124/mol.105.021832.

Kolluri, Siva Kumar, Un-Ho Jin, and Stephen Safe. 2017. “Role of the Aryl Hydrocarbon Receptor in Carcinogenesis and Potential as an Anti-Cancer Drug Target.” *Archives of Toxicology* 91 (7): 2497–2513.

Larigot, Lucie, Ludmila Juricek, Julien Dairou, and Xavier Coumoul. 2018. “AhR Signaling Pathways and Regulatory Functions.” *Biochimie Open* 7 (December): 1–9.

Lawson, Andrew R. J., Federico Abascal, Tim H. H. Coorens, Yvette Hooks, Laura O’Neill, Calli Latimer, Keiran Raine, et al. 2020. “Extensive Heterogeneity in Somatic Mutation and Selection in the Human Bladder.” *Science* 370 (6512): 75–82.

Lenis, Andrew T., Patrick M. Lec, Karim Chamie, and M. D. Mshs. 2020. “Bladder Cancer: A Review.” *JAMA: The Journal of the American Medical Association* 324 (19): 1980–91.

Loriot, Yohann, Andrea Necchi, Se Hoon Park, Jesus Garcia-Donas, Robert Huddart, Earle Burgess, Mark Fleming, et al. 2019. “Erdafitinib in Locally Advanced or Metastatic Urothelial Carcinoma.” *The New England Journal of Medicine* 381 (4): 338–48.

Love, Michael I., Wolfgang Huber, and Simon Anders. 2014. “Moderated Estimation of Fold Change and Dispersion for RNA-Seq Data with DESeq2.” *Genome Biology* 15 (12): 550.

Mullenders, Jasper, Evelien de Jongh, Anneta Brousali, Mieke Roosen, Jan P. A. Blom, Harry Begthel, Jeroen Korving, et al. 2019. “Mouse and Human Urothelial Cancer Organoids: A Tool for Bladder Cancer Research.” *Proceedings of the National Academy of Sciences of the United States of America* 116 (10): 4567–74.

Nakauma-González, J. Alberto, J. Alberto Nakauma-González, Maud Rijnders, Job van Riet, Michiel S. van der Heijden, Jens Voortman, Edwin Cuppen, et al. 2021. “Molecular Characterization Reveals Genomic and Transcriptomic Subtypes of Metastatic Urothelial Carcinoma.” bioRxiv 2021.03.17.435757.

Pandini, Alessandro, Michael S. Denison, Yujuan Song, Anatoly A. Soshilov, and Laura Bonati. 2007. “Structural and Functional Characterization of the Aryl Hydrocarbon Receptor Ligand Binding Domain by Homology Modeling and Mutational Analysis.” *Biochemistry* 46 (3): 696–708.

Priestley, Peter, Jonathan Baber, Martijn P. Lolkema, Neeltje Steeghs, Ewart de Bruijn, Charles Shale, Korneel Duyvesteyn, et al. 2019. “Pan-Cancer Whole-Genome Analyses of Metastatic Solid Tumours.” *Nature* 575 (7781): 210–16.

Robertson, A. Gordon, Jaegil Kim, Hikmat Al-Ahmadie, Joaquim Bellmunt, Guangwu Guo, Andrew D. Cherniack, Toshinori Hinoue, et al. 2018. “Comprehensive Molecular Characterization of Muscle-Invasive Bladder Cancer.” *Cell* 174 (4): 1033.

Santos, Catarina P., Eleonora Lapi, Jaime Martínez de Villarreal, Laura Álvaro-Espinosa, Asunción Fernández-Barral, Antonio Barbáchano, Orlando Domínguez, et al. 2019. “Urothelial Organoids Originating from Cd49f Mouse Stem Cells Display Notch-Dependent Differentiation Capacity.” *Nature Communications* 10 (1): 4407.

Seok, Seung-Hyeon, Woojong Lee, Li Jiang, Kaivalya Molugu, Aiping Zheng, Yitong Li, Sanghyun Park, Christopher A. Bradfield, and Yongna Xing. 2017. “Structural Hierarchy Controlling Dimerization and Target DNA Recognition in the AHR Transcriptional Complex.” *Proceedings of the National Academy of Sciences of the United States of America* 114 (21): 5431–36.

Shale, Charles, Jonathan Baber, Daniel L. Cameron, Marie Wong, Mark J. Cowley, Anthony T. Papenfuss, Edwin Cuppen, and Peter Priestley. 2020. “Unscrambling Cancer Genomes via Integrated Analysis of Structural Variation and Copy Number.” BioRxiv 2020.12.03.410860.

Shi, Ming-Jun, Xiang-Yu Meng, Jacqueline Fontugne, Chun-Long Chen, François Radvanyi,

and Isabelle Bernard-Pierrot. 2020. “Identification of New Driver and Passenger Mutations within APOBEC-Induced Hotspot Mutations in Bladder Cancer.” *Genome Medicine* 12 (1): 85.

Shimizu, Y., Y. Nakatsuru, M. Ichinose, Y. Takahashi, H. Kume, J. Mimura, Y. Fujii-Kuriyama, and T. Ishikawa. 2000. “Benzo[a]pyrene Carcinogenicity Is Lost in Mice Lacking the Aryl Hydrocarbon Receptor.” *Proceedings of the National Academy of Sciences of the United States of America* 97 (2): 779–82.

Supek, Fran, Matko Bošnjak, Nives Škunca, and Tomislav Šmuc. 2011. “REVIGO Summarizes and Visualizes Long Lists of Gene Ontology Terms.” *PloS One* 6 (7): e21800.

Vogel, Christoph Franz Adam, Wen Li, Dalei Wu, Jamie K. Miller, Colleen Sweeney, Gwendal Lazennec, Yasuko Fujisawa, and Fumio Matsumura. 2011. “Interaction of Aryl Hydrocarbon Receptor and NF-κB Subunit RelB in Breast Cancer Is Associated with Interleukin-8 Overexpression.” *Archives of Biochemistry and Biophysics* 512 (1): 78–86.

Wang, Zhongyan, Megan Snyder, Jessica E. Kenison, Kangkang Yang, Brian Lara, Emily Lydell, Kawtar Bennani, et al. 2020. “How the AHR Became Important in Cancer: The Role of Chronically Active AHR in Cancer Aggression.” *International Journal of Molecular Sciences* 22 (1).

Wilson, Shelly R., Aditya D. Joshi, and Cornelis J. Elferink. 2013. “The Tumor Suppressor Kruppel-like Factor 6 Is a Novel Aryl Hydrocarbon Receptor DNA Binding Partner.” *The Journal of Pharmacology and Experimental Therapeutics* 345 (3): 419–29.

Xie, Guofeng, Zhongsheng Peng, and Jean-Pierre Raufman. 2012. “Src-Mediated Aryl Hydrocarbon and Epidermal Growth Factor Receptor Cross Talk Stimulates Colon Cancer Cell Proliferation.” *American Journal of Physiology-Gastrointestinal and Liver Physiology*.

Xing, Yongna, Manabu Nukaya, Kenneth A. Satyshur, Li Jiang, Vitali Stanevich, Elif Nihal Korkmaz, Lisa Burdette, Gregory D. Kennedy, Qiang Cui, and Christopher A. Bradfield. 2012. “Identification of the Ah-Receptor Structural Determinants for Ligand Preferences.” *Toxicological Sciences: An Official Journal of the Society of Toxicology* 129 (1): 86–97.

Yu, Guangchuang, Li-Gen Wang, Yanyan Han, and Qing-Yu He. 2012. “clusterProfiler: An R Package for Comparing Biological Themes Among Gene Clusters.” *OMICS: A Journal of Integrative Biology*.

Yu, Zhenyuan, Jinling Liao, Yang Chen, Chunlin Zou, Haiying Zhang, Jiwen Cheng, Deyun Liu, et al. 2019. “Single-Cell Transcriptomic Map of the Human and Mouse Bladders.” *Journal of the American Society of Nephrology: JASN* 30 (11): 2159–76.

Zhao, Bin, Danica E. DeGroot, Ai Hayashi, Guochun He, and Michael S. Denison. 2010. “CH223191 Is a Ligand-Selective Antagonist of the Ah (Dioxin) Receptor.” *Toxicological Sciences*.

Zhu, Anqi, Joseph G. Ibrahim, and Michael I. Love. 2019. “Heavy-Tailed Prior Distributions for Sequence Count Data: Removing the Noise and Preserving Large Differences.” *Bioinformatics* 35 (12): 2084–92.

679 Figure 1

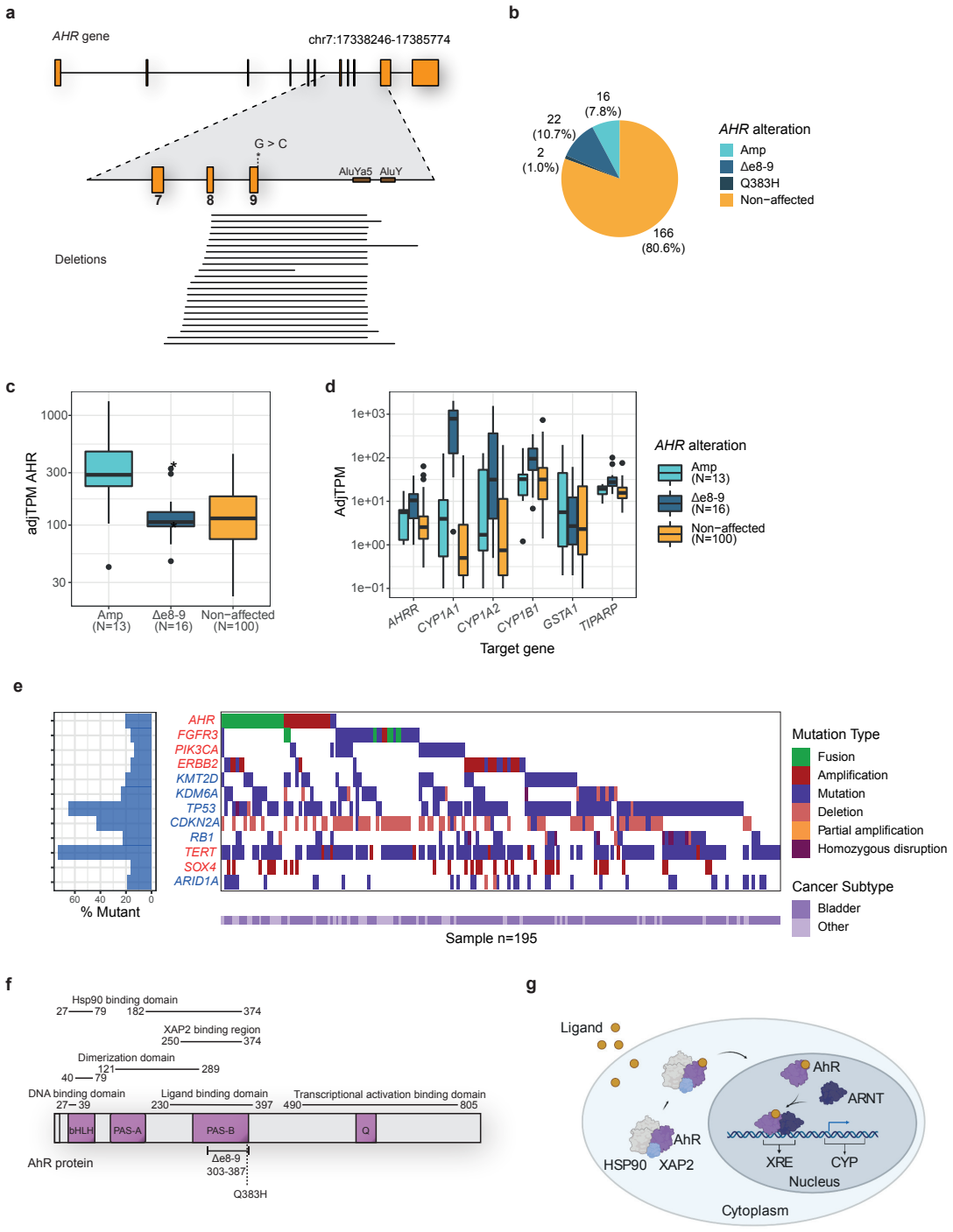

680

681 Figure 2

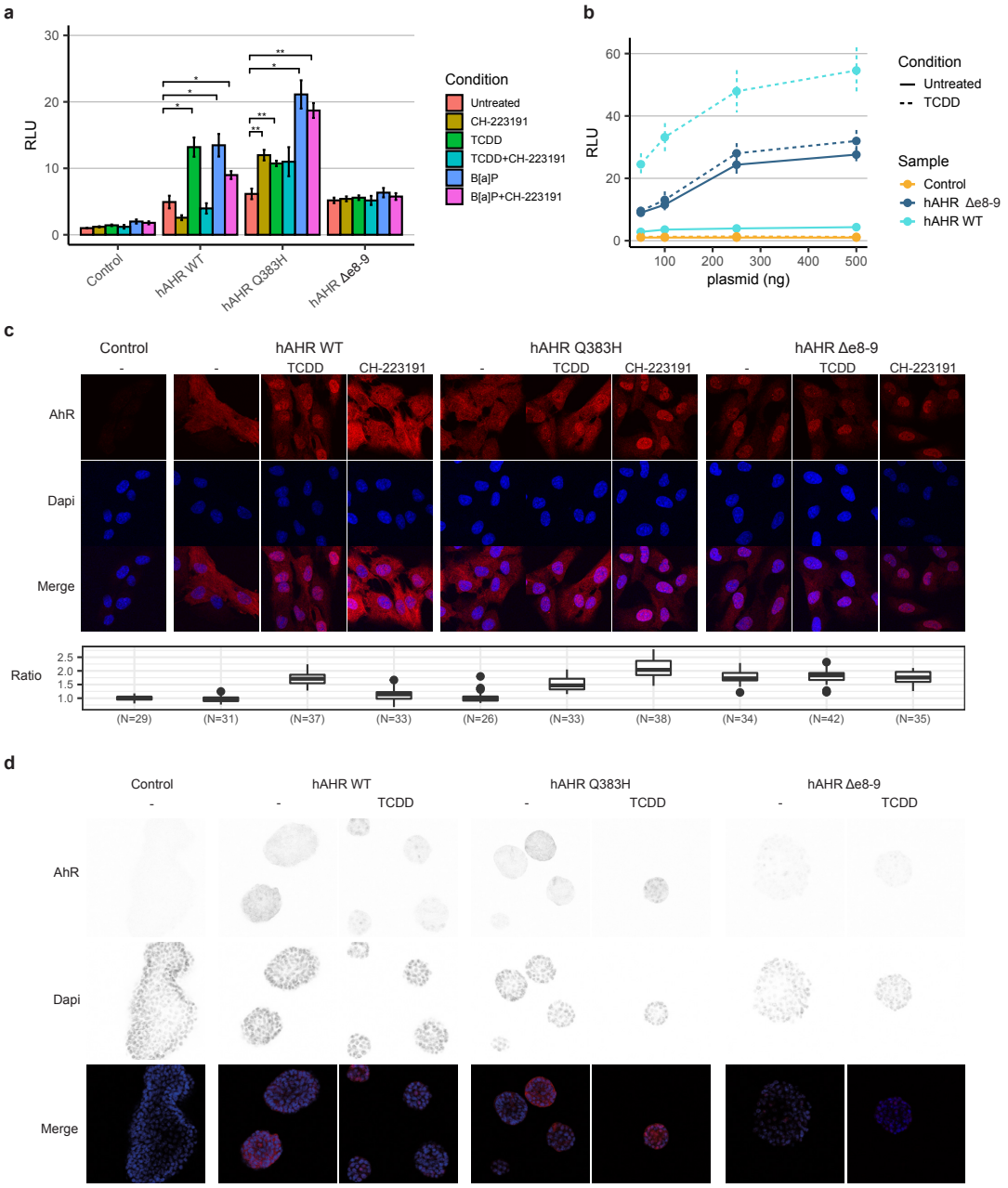

682

683 Figure 3

684

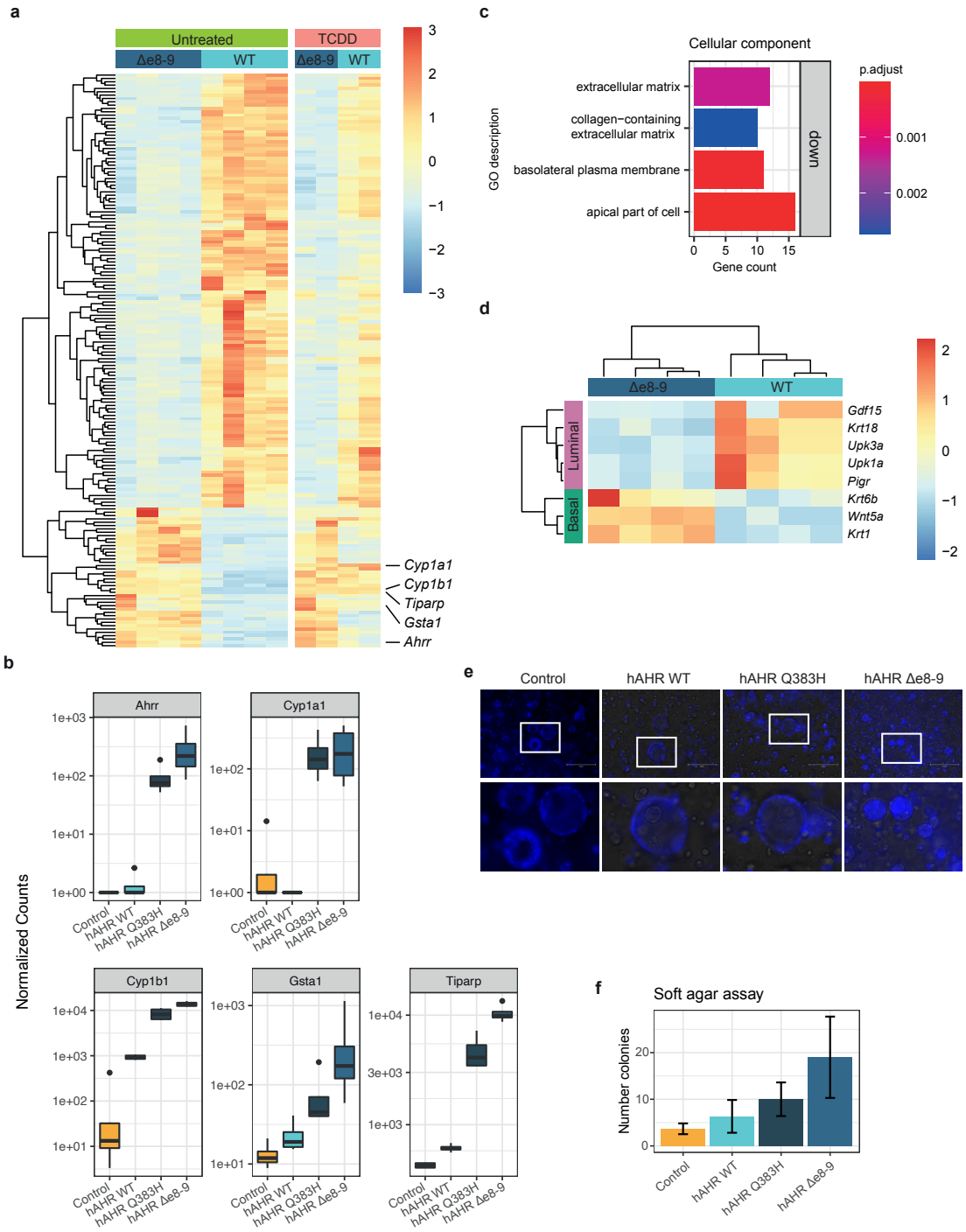
a
Untreated
TCDD
Δe8-9
WT
Δe8-9
WT
3
2
1
0
−1
−2
−3
Cyp1a1
Cyp1b1
Tiparp
Gsta1
Ahrr
c
Cellular component
GO description
extracellular matrix
collagen−containing extracellular matrix
basolateral plasma membrane
apical part of cell
down
0
5
10
15
Gene count
p.adjust
0.001
0.002
d
Δe8-9
WT
Luminal
Basal
Gdf15
Krt18
Upk3a
Upk1a
Pigr
Krt6b
Wnt5a
Krt1
2
1
0
−1
−2
b
Normalized Counts
Ahrr
Cyp1a1
Cyp1b1
Gsta1
Tiparp
1e+03
1e+02
1e+01
1e+00
1e+04
3e+03
Control
hAHR WT
hAHR Q383H
hAHR Δe8-9
e
Control
hAHR WT
hAHR Q383H
hAHR Δe8-9
f
Soft agar assay
Number colonies
20
10
0
Control
hAHR WT
hAHR Q383H
hAHR Δe8-9

685

686 Supplementary Figure 1

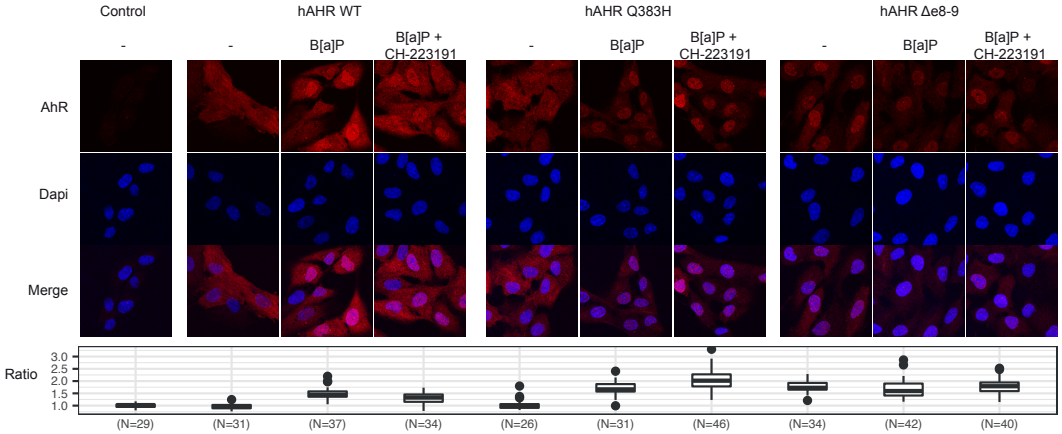

687